Rigler, R., & Ehrenberg, M. (1973) *Q. Rev. Biophys. 6*, 139–199.
Robbins, R. J., Fleming, G. R., Beddard, G. S., Robinson, G. W., Thistlethwaite, P. J., & Woolfe, G. J. (1980) *J. Am. Chem. Soc. 102*, 6271–6279.
Ross, J. B. A. (1976) Ph.D. Thesis, University of Washington, Seattle, WA.
Ross, J. B. A., Rousslang, K. W., Deranleau, D. A., & Kwiram, A. L. (1977) *Biochemistry 16*, 5398–5402.
Ross, J. B. A., Rousslang, K. W., de Haen, C., Lavis, V., & Deranleau, D. A. (1979) *Biochim. Biophys. Acta 576*, 372–384.
Ross, J. B. A., Rousslang, K. W., & Kwiram, A. L. (1980) *Biochemistry 19*, 876–883.
Ross, J. B. A., Schmidt, C., & Brand, L. (1981) *Biochemistry* (following paper in this issue).
Schiller, P. (1972) *Proc. Natl. Acad. Sci. U.S.A. 69*, 975–979.
Schneider, A. B., & Edelhoch, H. (1972a) *J. Biol. Chem. 247*, 4986–4991.
Schneider, A. B., & Edelhoch, H. (1972b) *J. Biol. Chem. 247*, 4992–4995.
Small, E. W., & Isenberg, I. (1977) *Biopolymers 16*, 1907–1928.
Szabo, A. G., & Rayner, D. M. (1980) *J. Am. Chem. Soc. 102*, 554–563.
Valeur, B., & Weber, G. (1977) *Photochem. Photobiol. 25*, 441–444.
Wahl, P. (1969) *Biochim. Biophys. Acta 175*, 55–64.
Wahl, P., Auchet, J.-C., & Donzel, B. (1974) *Rev. Sci. Instrum. 45*, 28–32.
Werner, T. C., & Forster, L. (1979) *Photochem. Photobiol. 29*, 905–914.

Time-Resolved Fluorescence of the Two Tryptophans in Horse Liver Alcohol Dehydrogenase†

J. B. Alexander Ross,‡ Carl J. Schmidt, and Ludwig Brand*

ABSTRACT: The tryptophan fluorescence decay of horse liver alcohol dehydrogenase, at 10 °C in 0.1 M pH 7.4 sodium phosphate buffer, with excitation at 295 nm, is a double exponential with time constants of 3.8 and 7.2 ns. Within experimental error, the two lifetimes remain constant across the emission spectrum. Only the 3.8-ns lifetime is quenched in the NAD^+–pyrazole ternary complex, and only the 7.2-ns lifetime is quenched by 0–0.05 M KI. On the basis of these results, we assign the 3.8-ns lifetime to the buried tryptophan, Trp-314, and the 7.2-ns lifetime to the exposed tryptophan, Trp-15. The steady-state lifetime-resolved emission spectrum of Trp-15 has a maximum at ~340 nm and that of Trp-15 is at ~325 nm. The total time-resolved emission, after 40 ns of decay, has a maximum between 338 and 340 nm and is primarily due to the Trp-15 emission. As a consequence of the wavelength dependence of the preexponential weighting factors, there is an increase in the average lifetime from the blue to the red edge of the emission. This increase reflects the change in the spectral contributions of Trp-15 and Trp-314. Consideration of the spectral overlap between the emission spectra of the two tryptophans and the absorption due to formation of the ternary complex, as well as the distances between the two residues and the bound NAD^+, shows that the selective fluorescence quenching in the ternary complex can be accounted for entirely by singlet–single energy transfer. The decay of the fluorescence anisotropy was measured as a function of temperature from 10 to 40 °C and is well described by a monoexponential decay law. Over this temperature range the calculated hydrodynamic radius increases from 33.5 to 35.1 Å. Evidently, the indole groups of Trp-15 and Trp-314 rotate with the protein as a whole, and there is some expansion of the protein matrix as the ambient temperature is increased.

Tryptophan fluorescence has been used as a sensitive probe for conformational perturbations in proteins and polypeptides. The emission maximum and intensity are often affected during events such as catalysis, denaturation, or intermolecular association. For example, a red shift in the spectrum is usually associated with an increase in the polarity of the local dielectric or with a quenching of the less solvent-accessible residues (Konev, 1967). In addition, collisional quenching has been used as an indicator of relative accessibility of tryptophans and to distinguish buried from exposed residues (Lehrer, 1971).

Interpretation of changes in the spectral parameters of multitryptophan proteins requires the identification of the affected residues. Time resolution of the fluorescence decay and its anisotropy has excellent potential for addressing this problem. Considerable improvements in methods of measurement and data analysis over the past decade [see review by Badea & Brand (1979)] make this approach feasible. However, since it has been found that a number of *single*-tryptophan proteins and polypeptides exhibit multiexponential decay kinetics (Grinvald & Steinberg, 1976), correlation of the fluorescence decay with individual tryptophan residues is not straightforward. In more complicated cases, such as that of pig heart lactate dehydrogenase which has six tryptophans, association of decay times with particular residues is tenous (Torikata et al., 1979). Nevertheless, progress has been made for proteins with two tryptophan residues. Privat et al. (1980) resolved the fluorescence decay of yeast 3-phosphoglycerate kinase into three components, two of which are attributed to one of the tryptophans. The single-exponential tryptophan has

† From the Department of Biology and McCollum-Pratt Institute, The Johns Hopkins University, Baltimore, Maryland 21218. *Received December 15, 1980.* Supported by National Institutes of Health Grant GM 11632. Contribution No. 1099 from the McCollum-Pratt Institute. A preliminary account of this work was presented at the annual meeting of the American Society for Photobiology held in Colorado Springs, CO, Feb 1980 (Abstr. No. P6).

‡ Present address: Department of Laboratory Medicine, University Hospital, University of Washington, Seattle, WA 98195.

0006-2960/81/0420-4369$01.25/0

the shortest lifetime (0.4–0.6 ns) and the more blue-shifted emission. The double-exponential tryptophan (3.1 and 7.0 ns) exhibits wavelength-independent kinetic parameters. Barboy & Feitelson (1978) have examined the decay kinetics of horse liver alcohol dehydrogenase (ADH)[1] and report two lifetimes of 2.2 and 5.7 ns. Quenching of the longer decay component with KI was interpreted in terms of conformational fluctuations allowing access to the buried tryptophan.

The purpose of this paper is to report the time-resolved fluorescence of the two tryptophan residues in free ADH and in the NAD^+–pyrazole ternary complex. We also examine the fluorescence anisotropy decay of the tryptophans. ADH is of special interest because much is known about its mechanism and physical structure [see review by Brändén et al. (1975)]. One of the tryptophans is well exposed to solvent (Trp-15), and the other is buried in a cage of hydrophobic residues (Trp-314) at the dimer interface between the identical 40 000 M_r subunits. The carbonyl oxygen of each Trp-314 is hydrogen bonded to the amide hydrogen of its twin residue. We have assigned the fluorescence decay parameters of Trp-15 and Trp-314 and have examined the mobility of their indole groups. Within experimental error the individual fluorescence decay times are essentially wavelength independent, the exposed residue having not only the more red-shifted time-resolved emission spectrum but also the longer lifetime. Since the buried and exposed tryptophans have shifted steady-state lifetime-resolved spectra, the average lifetime of ADH increases across the total emission spectrum. And finally, the indole groups of ADH appear to rotate with the protein as a whole, not independently as observed by Munro et al. (1979) for several other proteins.

Experimental Procedures

Materials. Horse liver alcohol dehydrogenase was obtained from Boehringer Mannheim as a crystalline suspension in 10% ethanol buffered at pH 7 with 0.02 M phosphate. NAD^+ was purchased from Sigma Chemical Co. Pyrazole and *p*-terphenyl were Aldrich products. *N*-Acetyltryptophanamide (NATA) was obtained from Vega. Spectrograde cyclohexane and 1,1′-binaphthyl were Eastman products. Other chemicals were reagent grade.

Enzyme Preparation. The enzyme was extensively dialyzed at 4 °C against 0.1 M phosphate pH 7.4 buffer. Material which remained undissolved at the end of dialysis was removed by centrifugation. The protein concentration was determined both by the absorbance at 280 nm (Sund & Theorell, 1963) and by the NAD^+ binding site titration in the presence of excess pyrazole (Theorell & Yonetani, 1963). The specific activity of the enzyme was measured, with the assay of Dalziel (1957), by following the absorbance change at 340 nm as NAD^+ is converted to NADH, with ethanol as substrate. Absorbance measurements were made on either a Cary 14 or a Cary 219 spectrophotometer. The difference between the number of sites determined by formation of the NAD^+ ternary complex with pyrazole and the number of sites converting ethanol to acetaldehyde was usually within 10%. Both methods showed similar agreement with the number of sites determined by the 280-nm absorbance. The ratio of the enzyme absorption at 280 nm to that at 260 nm was ~1.4. The activity of the enzyme was checked periodically and found to be constant during the 3–4 weeks a particular preparation was being used.

Fluorescence Quenching. Fluorescence quenching of ADH was carried out either with NAD^+ and pyrazole or with KI. Solutions of KI contained $\sim 10^{-4}$ M sodium sulfite to inhibit formation of I_3^- (Lehrer, 1971). All solutions were kept refrigerated, and care was taken to avoid their exposure to room light.

Fluorescence Spectroscopy. Steady-state and nanosecond decay measurements were carried out as described in the preceding paper (Ross et al., 1981). The anisotropy decay measurements were carried out, however, in the fashion described by Dale et al. (1977). According to this method, Correction for polarization errors was minimized by use of the quarter-wave plate in the excitation path. This correction, the "*G*-factor", appears in the expression for the decay of the emission anisotropy as

$$r(t) = \frac{I_{VV}(t)G - I_{HV}(t)}{I_{VV}(t)G + 2I_{HV}(t)} \quad (1)$$

where $G = I_{HH}/I_{VH}$ and the first and second subscripts refer to the excitation and emission (Paoletti & Le Pecq, 1969; Azumi & McGlynn, 1962). The value of G was determined in a separate experiment by rotating the emission polarizer from the vertical to the horizontal and then measuring the steady-state intensities of I_{HH} and I_{VH}. A separate lifetime experiment with the single exponential standard provided the time shift for the sample decay curves.

Analysis of Fluorescence Decay Data. The decay of the fluorescence emission may be complex. If a multiexponential law is assumed, the impulse response is

$$I(t) = \sum_i \alpha_i \exp(-t/\tau_i) \quad (2)$$

where α_i is the relative weight and τ_i is the decay constant for the ith component. Similarly, the decay of the fluorescence anisotropy for nonspherical rotors is complex (Perrin, 1934, 1936; Tao, 1969) but may in general be treated as a sum of exponentials [see Rigler & Ehrenberg (1973) and Small & Isenberg (1977)]. Thus, the time-dependent anisotropy is

$$r(t) = \sum_j \beta_j \exp(-t/\phi_j) \quad (3)$$

where the zero-point anisotropy is determined by the sum of the preexponential terms β_j and ϕ_j are the rotational correlation times. The decay of the emission anisotropy, $r(t)$, was derived by first analyzing the sum curve

$$s(t) = I_{VV}(t)G + 2I_{HV}(t) \quad (4)$$

and the difference decay curve

$$d(t) = I_{VV}(t)G - I_{HV}(t) \quad (5)$$

according to the relationship

$$r(t) = d(t)/s(t) \quad (6)$$

The lifetime impulse response parameters were first determined by analysis of $s(t)$. Then the parameters for $r(t)$ were recovered from analysis of the difference curve $d(t)$, assuming a model in which the decay of the emission anisotropy is the same for all the kinetic components in the total emission (Dale et al., 1977; Wahl, 1969). So

$$d(t) = [\sum_i \alpha_i \exp(-t/\tau_i)][\sum_j \beta_j \exp(-t/\phi_j)] \quad (7)$$

If there are two or more emitting species, each with different rotational properties, then the observed difference decay is an average (Chen et al., 1977), where

$$\langle d(t) \rangle = \sum_i r_i(t)s_i(t) = \sum_i d_i(t) \quad (8)$$

The partial difference decays $d_i(t)$ are related to the sum and

[1] Abbreviations used: ADH, horse liver alcohol dehydrogenase; ACTH-(1–24), adrenocorticotropin-(1–24); NATA, *N*-acetyltryptophanamide; NAD^+, nicotinamide adenine dinucleotide; ODMR, optical detection of magnetic resonance; TRES, time-resolved emission spectrum.

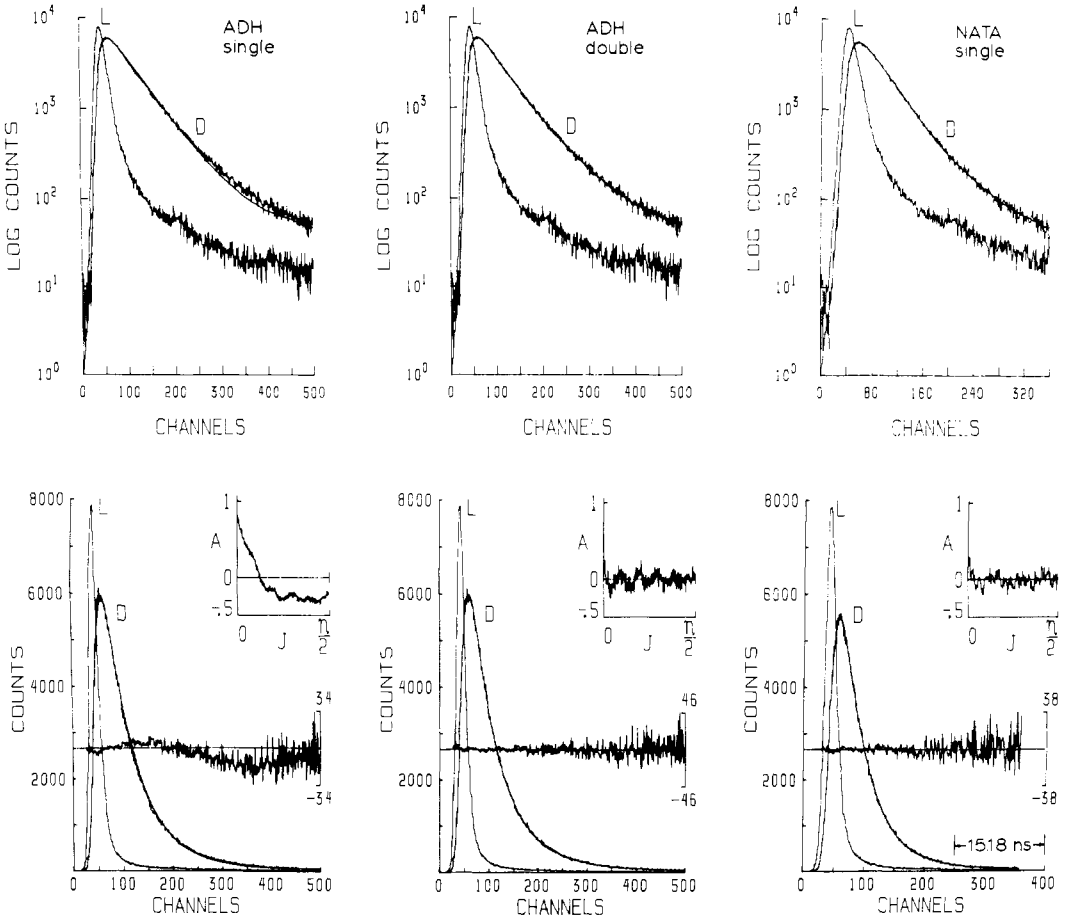

FIGURE 1: Fluorescence decay data of 8×10^{-5} M ADH and 1×10^{-4} M NATA in 0.1 M sodium phosphate buffer at 10 °C. The decay curves (D) are shown, along with the experimental lamp (L), in both semilogarithmic (top row) and linear form (bottom row). Included in the linear representation are the percent residuals and their autocorrelation. The solid noise-free line represents the theoretical parameters convolved with the lamp. With natural light excitation at 295 nm (bandwidth of 10.6 nm) and the emission monitored at 350 nm (bandwidth of 6.6 nm), the best fits to the data from left-to-right were respectively: for ADH as a single, $\tau = 5.40$ ns, with $\chi^2 = 3.02$, and as a double, $\tau_1 = 3.90$ ns, $\alpha_1 = 0.601$, $\tau_2 = 6.92$, $\alpha_2 = 0.399$, with $\chi^2 = 1.14$; for NATA, $\tau = 3.79$ ns, with $\chi^2 = 1.27$.

emission anisotropy decays $s_i(t)$ and $r_i(t)$ by eq 6.

A nonlinear least-squares method was used to analyze the decay curves (Grinvald & Steinberg, 1974). The fit between the theoretical curve and the data was evaluated from the percent residuals, the autocorrelation function of the residuals, and the reduced χ^2. The variances $\sigma^2(t) = [I_{VV}(t)G]^2 + 4I_{HV}(t)$ and $\sigma^2(t) = [I_{VV}(t)G]^2 + I_{HV}(t)$ were used for appropriate statistical weighting of the sum and difference curves, respectively. Simulations of the data were constructed from the derived parameters, as well as from hypothetical parameters, to determine the reliability of any supposed model.

Energy Transfer Calculations. Singlet–singlet energy transfer, which is essentially due to electronic dipole–dipole coupling, has a sixth power dependence upon the separation between the donor and acceptor (Förster, 1948, 1951). The distance, R_0, for 50% transfer efficiency is described by

$$R_0 = [(8.79 \times 10^{-25} \text{ mmol})\kappa^2\phi_D n^{-4} J]^{1/6} \quad (9)$$

in which κ is the orientation factor for the resonance interaction, ϕ_D is the quantum yield of the donor in the absence of energy transfer, n is the refractive index of the medium, and

$$J = \int_0^\infty F_D(\lambda)E_A(\lambda)\lambda^4 \, d\lambda \quad (10)$$

is the overlap integral between the normalized (to unity) fluorescence emission of the donor, F_D, and the molar decadic extinction coefficient of the acceptor, E_A. The efficiency of energy transfer to NAD^+ from the two tryptophan residues can be calculated from their lifetimes prior to and subsequent to ternary complex formation. Following the relationships developed by Eisinger (1969) and Schiller (1972), the efficiency of transfer E_T over a distance R is

$$E_T = \frac{(R_0/R)^6}{[(R_0/R)^6 + 1]} = \frac{(\tau_D^0 - \tau_D)}{\tau_D^0} \quad (11)$$

where τ_D^0 is the lifetime of the donor including all nonradiative processes except energy transfer and τ_D is the lifetime in the presence of the acceptor.

Results

Fluorescence Decay of Tryptophan in ADH. The fluorescence decay data of ADH fit for a single- and for a double-exponential are shown in Figure 1, along with the single-exponential standard NATA. The top and bottom graphs in the figure are respectively semilogarithmic and linear representations of the data. The theoretical curve obtained by convolving the best parameters for a single exponential of 5.09 ns clearly fails to fit the ADH data at long times in the semilogarithmic plot. Furthermore, trends in the percent residuals and in their autocorrelation in the linear plot indicate large systematic deviations between the data and the theoretical curve. However, a double-exponential decay law provides a superior theoretical fit for the same data. It should be noted that χ^2 for the ADH single-exponential fit is 3.02 whereas for the double it is 1.14, and the single-exponential fit for the NATA data has a χ^2 of 1.27. Analysis of the ADH data for a triple exponential gave no improvement in χ^2, and two of the three lifetimes were identical. Therefore, by our

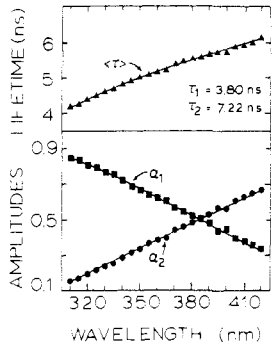

FIGURE 2: Lifetimes and relative amplitudes of ADH as a function of the fluorescence emission spectrum. The average lifetime $\langle\tau\rangle$ was calculated according to eq 9. These values are comparable with the average lifetime obtained by phase fluorometry, provided the product of the lifetime and modulation frequency are much less than unity [Inokuti & Hirayama (1965) and references cited therein]. Data were collected under the condition specified in Figure 1.

criteria, the fluorescence decay is most accurately described as a double exponential.

Fluorescence decay data (53 data sets) were obtained over the wavelength region of 310–420 nm taken each 5 nm. The data were analyzed in two ways by the method of nonlinear least squares. First, the analysis was in terms of a double exponential with τ_1, τ_2, α_1, and α_2 allowed to run free. This gave values of $\tau_1 = 3.6 \pm 0.4$ ns and $\tau_2 = 7.1 \pm 0.6$ ns. There was no evidence for any wavelength dependence in τ_1. There was a small increase in τ_2 (as a function of wavelength), but this was almost lost within the noise of the τ_2 values. It is difficult to obtain a reasonable recovery of double-exponential decay parameters when the ratio of the lifetimes is <2 (Gafni et al., 1975). The present situation is thus a borderline case. We elected an alternative approach. A nonlinear least-squares analysis was performed, but the vallues of τ_1 and τ_2 were fixed at 3.80 and 7.22 ns, and the values of α_1 and α_2 were allowed to run free during the analysis. The analyses obtained under these conditions gave fits that were excellent according to the χ^2, the residuals, and the autocorrelation of the residuals. The results of this analysis are shown in Figure 2. The mean lifetime as used here is defined as follows (Inokuti & Hirayama, 1965):

$$\langle\tau\rangle = \frac{\int_0^\infty tI(t)\,dt}{\int_0^\infty I(t)\,dt} = \frac{\sum_i \alpha_i\tau_i^2}{\sum_i \alpha_i\tau_i} \qquad (12)$$

This definition of mean decay time is close to the mean lifetime obtained in a phase experiment. Replicate experiments obtained at any one wavelength showed excellent precision in the mean lifetime. Furthermore, the same mean lifetimes were obtained by either way of analyzing the data. It is clear that the change in average lifetime with wavelength has its origin in the variation of amplitudes.

Time-Resolved Emission Spectrum of ADH. Deconvolved time-resolved emission spectra (TRES) (Easter et al., 1976) were generated according to the two models in which τ_1 is 3.80 ns for all wavelengths and either τ_2 is constant at 7.22 ns or increases monotonically from 6.50 ns at 310 nm to 7.95 ns at 420 nm. The impulse responses $f(\lambda,t)$ at 5-nm increments were normalized to the corrected steady-state spectrum $F(\lambda)$, obtained under the same optical conditions. Defining $h(\lambda)$ as

$$h(\lambda) = F(\lambda)/\int_0^\infty f(\lambda,t)\,dt \qquad (13)$$

the properly normalized TRES is

$$I(\lambda,t) = h(\lambda)f(\lambda,t) \qquad (14)$$

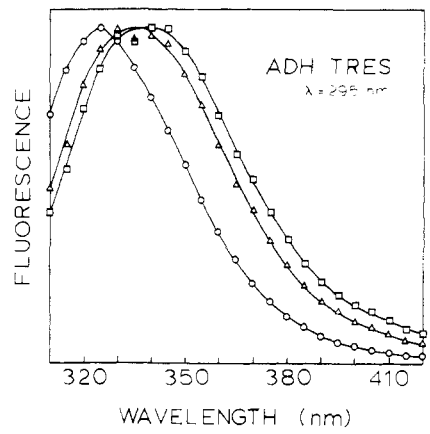

FIGURE 3: Time-resolved emission spectra of ADH at 10 °C in 0.1 M sodium phosphate buffer, obtained under the optical conditions described in Figure 1. The spectra were corrected by using NATA as a reference: steady-state spectra of ADH and NATA were collected on the lifetime instrument, the optical configuration remaining the same as when collecting the decay data. The three spectra are at the effective zero time (○), after 40 ns of decay with τ_2 fixed at 7.22 ns (△), and with τ_2 varied monotonically from 6.50 ns at 310 nm to 7.95 ns at 420 nm (□). In both cases, τ_1 was held constant at 3.80 ns. The zero-time spectra obtained from the two models are indistinguishable.

where $I(\lambda,t)$, is a surface representing the intensity at all wavelengths and times during the fluorescence decay. The *peak* normalized TRES, obtained in this fashion, is shown for two time windows in Figure 3. The first is at the effective zero time, the instant after excitation, and the second is following 40 ns of decay. After this interval, the remaining intensity of the *short*-lived component is ~1% of the total emission. Therefore, the 40-ns spectrum is almost entirely due to the long lifetime. When τ_2 is constant, this spectrum has a maximum at ~338 nm with a bandwith (full width at half-height) of about 58 nm. When τ_2 varies, the maximum is at 340 nm, and the bandwidth is nearly 60 nm. Also with the same optical configuration, the corrected steady-state emission maximum of NATA is at 350 nm with a bandwidth of 60 nm.

Fluorescence Quenching. With excitation at 295 nm, both Trp-15 and Trp-314 contribute to the ADH emission (Rousslang et al., 1978, 1979). With excitation further to the red, the contribution of Trp-15 diminishes, leaving Trp-314 as the dominant emitter (Purkey & Galley, 1970). We measured the fluorescence decay of ADH, shifting the excitation from 295 to 313 nm (λ_{em} = 380 nm) and found that the normalized amplitude of the *short* component, monitored toward the red edge of the spectrum at 380 nm, increased from 0.55 to 0.83. This observation indicated that the likely origin of the short lifetime was indeed Trp-314. To test this hypothesis, we carried out two kinds of fluorescence quenching experiments designed to distinguish between the relative contributions of Trp-15 and Trp-314 to the total emission. First, we used KI which has been demonstrated to preferentially quench exposed tryptophan residues (Lehrer, 1971). Second, we measured the fluorescence decay of the NAD^+–pyrazole ternary complex. Whereas KI quenches the *red* portion of the spectrum, implicating the preferential quenching of Trp-15 to Trp-314 (Abdallah et al., 1978; Laws & Shore, 1978), the *blue* portion is quenched in the ternary complex.

We predicted that in the quenching with KI, at increasing concentrations of iodide, the long-lived fluorescence component τ^2 would be primarily affected. Since, according to this hypothesis, the two lifetimes would then converge, become the same, and then diverge, the χ^2 obtained by analyzing the data

Table I: Decay Parameters for Tryptophan Emission Anisotropy of ADH[a]

	fluorescence decay parameters					hydrodynamic parameters				
T (°C)	α_1	τ_1 (ns)	α_2	τ_2 (ns)	$\langle\tau\rangle$ (ns)	ϕ (ns)	r_0	$\langle r\rangle$	η (cP)	R (Å)
10.0	0.74	4.2	0.26	7.8	5.63	56	0.210	0.190	1.385	33.5
27.5	0.73	3.8	0.27	7.0	5.09	36	0.207	0.182	0.894	34.2
40.0	0.72	3.4	0.28	6.0	4.49	29	0.200	0.174	0.695	35.1
precision:	±0.05	±0.1	±0.05	±0.2	±0.03	±1.5	±0.005	±0.003		

[a] Emission at 350 nm with an 8.3-nm band-pass. The fluorescence lifetimes were obtained from analysis of $I_{VV}G + 2I_{VH}$. The G factor was determined by measuring I_{HH} and I_{HV} under steady-state counting conditions. The average lifetime $\langle\tau\rangle$ is defined as $\Sigma_i\alpha_i\tau^2/\Sigma_i\alpha_i\tau_i$ (Inokuti & Hirayama, 1965). The values for η were determined by Professor D. C. Teller. A pH 7.4 sodium phosphate buffer was used. The fluorescence data are the average of triplicate measurements at each temperature on the same sample.

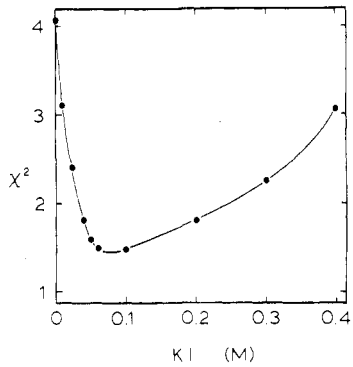

FIGURE 4: Plot of χ^2 obtained from fitting fluorescence decay of ADH as a function of KI concentration to a single exponential. KI was added in sequential aliquots to an 8×10^{-5} M ADH solution, and the emission was monitored at 360 nm. The other experimental conditions were as specified in Figure 1.

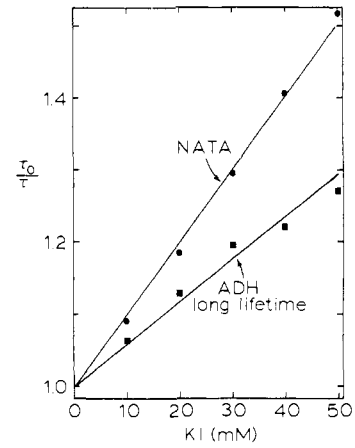

FIGURE 5: Stern–Volmer plot of quenching of 360-nm fluorescence decay of NATA (●) and long-lived decay component of ADH (■) by 0–0.05 M KI at 10 °C. The respective quenching constants for NATA and the long ADH lifetime are 10.28 and 5.51 M^{-1}. The other conditions are as described in Figure 1.

for a single exponential should fit a concave curve as a function of KI concentration. On the other hand, we expected that the quenching of the tryptophan fluorescence by formation of the NAD^+–pyrazole complex would change the decay parameters of the short-lived component (τ_1) and that the decay parameters of the long-lived component should only be minimally perturbed.

Figure 4 depicts the change in χ^2 for a single exponential fit of the fluorescence decay as a function of KI concentration. The emission was monitored at 360 nm, and the temperature was maintained at 10 °C. A distinct minimum is observed for the χ^2 values between 60 and 100 mM KI. If the data for the KI concentration ranging up to 30 mM are analyzed for a double exponential, only the long lifetime (τ_2) decreases. At ~40 mM KI, reproducible values for the two separate lifetimes can no longer be extracted from the data. Presumably, due to the selective quenching, the long decay component no longer differs much from the short one.

In conjunction with the decay experiments, we also examined the steady-state spectral dependence of quenching with KI. Barboy & Feitelson (1978) and Lakowicz & Cherek (1980) rely upon the assumption that with excitation at 300 nm the relative contribution of Trp-15 to the fluorescence is negligible. In the concentration range of 0–50 mM KI and with excitation at 300 or 305 nm, there is no significant quenching at the blue edge of the fluorescence (320 nm) while there is obvious quenching at the red edge (380 nm). The band-pass for excitation was 2 nm, and the band-pass for emission was 8 nm. This experiment provides evidence that both the buried and exposed tryptophan residues are excited at 300–305 nm.

On the basis of the above information, we suggest (a) that only the blue tryptophan is associated with the short fluorescence lifetime and (b) that this residue is also not affected by KI in the range of 0–50 mM. We reanalyzed the quenching data, holding the short lifetime constant at 3.80 ns. Graphing the lifetime value of the long-lived decay component in the absence of KI divided by its lifetime as a function of KI, we obtained a linear Stern–Volmer plot in the concentration range up to 50 mM KI (Figure 5). With $\tau_2 = 7.22$ ns at 360 nm, the bimolecular quenching constant is 7.6×10^8 M^{-1} s^{-1}. Under the same experimental conditions, the bimolecular quenching constant for NATA is 2.85×10^9 M^{-1} s^{-1}, which agrees with the value of 2.9×10^9 M^{-1} s^{-1} obtained by Barboy & Feitelson (1978).

Experiments were done to compare the fluorescence decay of the ADH ternary complex with NAD^+ and pyrazole to that found with the free enzyme. Pyrazole itself has no significant effect on the fluorescence decay times of the enzyme. Saturation of the active sites as a ternary complex decreased only the short decay time, τ_1. With emission at 350 nm, τ_1 went from 3.8 (free enzyme) to 2.4 (ternary complex) ns with no change in τ_2 which remained at 7.2 ns. It is of interest to point out that an analysis with all the decay parameters allowed to vary gave excellent results here ($\tau_1 = 2.39 \pm 0.04$ ns, $\tau_2 = 7.20 \pm 0.07$ ns) for a triplicate data set. This is in contrast to the results with the free enzyme and is attributed to the increased ratio of τ_2 to τ_1. The decay constants obtained with the ternary complex showed no dependence on emission wavelength from 320 to 380 nm.

Rotational Relaxation of Trp-15 and Trp-313. The decay of the fluorescence anisotropy of ADH was measured at 10, 27.5, and 40 °C. The steady-state anisotropies measured on the MPF-4 fluorometer agreed within experimental error with the values calculated by using the lifetime instrument G factor and the integrated decay curves I_{VV} and I_{HV}. The fluorescence lifetime (from the sum analysis) and anisotropy parameters (from the difference analysis) as a function of temperature are listed in Table I. Included in this table is the hydrody-

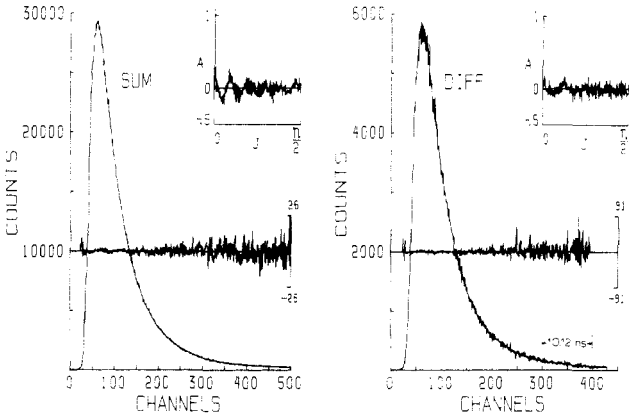

FIGURE 6: Linear presentation of sum ($I_{VV}G + 2I_{VH}$) and difference data ($I_{VV}G - I_{VH}$) of 8×10^{-5} M ADH in 0.1 M phosphate buffer at 10 °C, with excitation at 295 nm and emission monitored at 350 nm (8-nm band-pass). The theoretical fit for the sum curve gave the following decay parameters: $\tau_1 = 4.16$ ns, $\alpha_1 = 0.71$, $\tau_2 = 7.58$ ns, $\alpha_2 = 0.29$, with $\chi^2 = 1.30$. The anisotropy parameters, obtained from the difference curve and the decay parameters of the sum curve according to the impulse response model $d(t) = r(t)s(t)$, yielded a single rotational correlation time of 56 ns and a zero-time anisotropy of 0.204 with $\chi^2 = 0.93$.

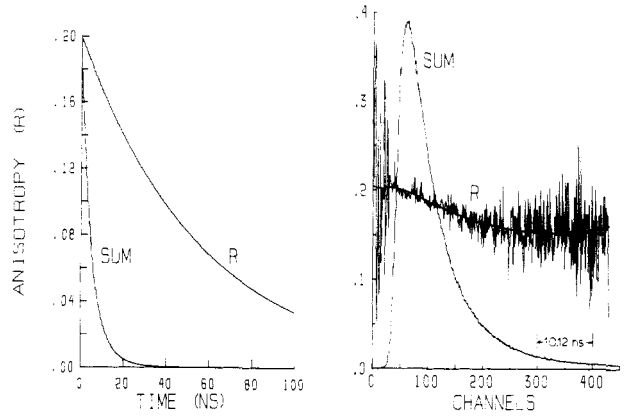

FIGURE 7: Convolved anisotropy data and their theoretical fit from parameters in Figure 6, compared with convolved total fluorescence decay from corresponding sum curve. The impulse response of the fluorescence decay and the theoretical anisotropy decay are also shown.

namic radius, calculated from the anisotropy parameters according to a homogenious spherical model. By use of the Einstein (1906) relationship for the Brownian rotation of dipoles

$$V = kT\phi/\eta \qquad (15)$$

in which V is the volume, k is Bolzmann's constant, and η is the viscosity. The rotational rates were determined from the sum and difference curves (Figure 6) as described under Experimental Procedures. The decay of the anisotropy, recovered from analysis of the difference curve, was best fit by a single-term exponential at all three temperatures. Examples of the convolved anisotropy decay and the convolved sum decay are shown in Figure 7 for comparison with the impulse responses derived from the sum and anisotropy decay parameters. Clearly the more accurate anisotropy information is obtained in the earlier part of the fluorescence decay. At later times, the poorer signal-to-noise ratio of the anisotropy decay is due to the low remaining fluorescence intensity. The results show that, within the error of measurement, the hydrodynamic radius of ADH increases slightly with temperature from 10 to 40 °C.

Discussion

Fluorescence Decay Model. Each subunit of horse liver alcohol dehydrogenase has two tryptophan residues. One of these (Trp-314) is buried while the other (Trp-15) is exposed to the solvent. We will now argue that each of the two observed decay constants has its origin in one of the two specific tryptophan residues. While the assignment of the decay constants of a system with a biexponential decay law to each of two fluorophores may seem to be self-evident, this is not the case.

A number of *single*-tryptophan proteins exhibit multiexponential decay kinetics (Grinvald & Steinberg, 1976). Therefore, a priori, there is no reason to assume that either Trp-15 or Trp-314 will emit according to a monoexponential decay law. Multiexponential decay kinetics for a single tryptophan residue could have its origin in ground-state microheterogeneity or in a variety of excited-state reactions. Dipolar relaxation around a fluorophore on the same time scale as the fluorescence decay can be the origin of complex decay.

Solvent relaxation kinetics lead to a red shift in the TRES at progressively longer times (DeToma et al., 1976). In addition, there is an increase in the mean lifetime $\langle\tau\rangle$ with increasing wavelength (Badea et al., 1978). In fact, the lifetime of ADH, excited at 300 nm, was observed by Lakowicz & Cherek (1980) to increase from the blue to the red edge of the fluorescence emission. These workers interpret their phase results in terms of dipolar reorientation around the excited indole ring of Trp-314.

A model that is consistent with our data is that the double-exponential kinetics arises from two different ground-state configurations (or distinct local environments) of the two ADH tryptophans. In this case, each residue would be expected to have a different emission spectrum, and the characteristic lifetime of each tryptophan would be invarient across the protein fluorescence. However, the preexponential terms would change according to the differing energy distributions of the two spectral envelopes.

A two-state excited-state reaction mechanism predicts similar double-exponential kinetics, with two wavelength-independent lifetimes but changing amplitudes for the emission of the initially excited molecule (Laws & Brand, 1979). If a significant fraction of the emission originated from a species formed in the excited state, then a negative preexponential term would be expected at the red edge of the fluorescence spectrum. Although this was not observed in our data, failure to detect a negative amplitude does not preclude the mechanism, since resolution of the kinetics also depends upon total spectral separation of the excited-state product and the parent excited molecule (Gafni et al., 1976).

It was pointed out in the results for the free enzyme that analysis of the data with α_1, τ_1, α_2, and τ_2 allowed to vary resulted in a small increase in τ_2 as a function of emission wavelength. However, in the ternary complex (when τ_1 was quenched) τ_1 and τ_2 were clearly independent of wavelength. The results of both analyses of the free enzyme data (fixing τ_1 and τ_2 *or* fixing τ_1 and allowing τ_2 to vary) are reflected in the TRES shown in Figure 3. The small wavelength dependence in τ_2 with the concomitant slight red shift in the TRES after 40 ns of decay could be due to solvent relaxation in the free enzyme. However, because the amplitudes and lifetimes are correlated in the analysis, there is no effect upon the mean lifetime, $\langle\tau\rangle$. In summary, the increase in the mean lifetime as a function of wavelength can be accounted for by the change in the preexponential terms according to the spectral distribution of the two tryptophans. Moreover, these

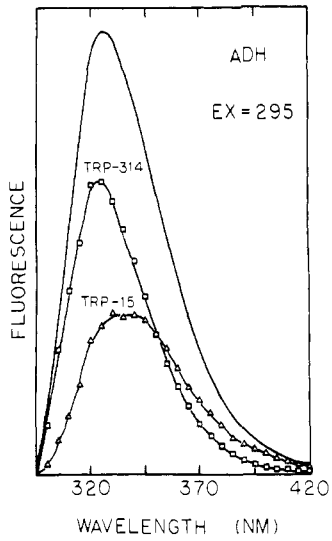

FIGURE 8: Steady-state fluorescence spectrum of ADH (same conditions as in Figure 1) resolved into fractional contributions of the 3.8-ns (□) and 7.2-ns (Δ) components. A summary of the resolved spectral parametes is given in Table II.

results can accommodate some solvent relaxation.

Considerable information is available regarding the spectroscopic characteristics of Trp-15 and Trp-314. The latter absorbs further to the red than Trp-15 (Purkey & Galley, 1970). However, it cannot be assumed that *only* Trp-314 is excited at 300 nm. J. B. A. Ross, K. W. Rousslang, and A. L. Kwiram (unpublished experiments) have observed phosphorescence (77 K) emission due to Trp-15 with excitation at 300 nm. Abdallah et al. (1978) have shown by using KI quenching that Trp-314 has a fluorescence maximum at 320 nm as compared to an emission at 340 nm for Trp-15. With excitation at 300 nm, we have observed more quenching with KI at the red edge of the emission than at the blue edge. This is consistent with the assertion that both tryptophan residues are excited at 300 nm.

Assignment of Tryptophan Decay Constants. Horse liver alcohol dehydrogenase shows double-exponential decay kinetics with time constants of 3.8 and 7.2 ns. The results are consistent with the assignment of the 7.2-ns decay to Trp-15 (exposed) and the 3.8-ns component to Trp-314 (buried). KI selectively quenches the 7.2-ns component as expected.

We have generated the spectra associated with the 3.8- and 7.2-ns decay components according to the relationship of Donzel et al. (1974)

$$F_i = F_{ss}(\alpha_i\tau_i/\sum_i \alpha_i\tau_i) \qquad (16)$$

where F_{ss} is the total steady-state spectrum, F_i is the spectrum associated with the ith component, and α_i, and τ_i are the fluorescence decay parameters. The resolved spectra associated with each decay time, and thus with Trp-15 and Trp-314, are shown in Figure 8 together with the total steady-state spectrum of the free enzyme. Abdallah et al. (1978) in an elegant paper used KI quenching experiments to resolve the steady-state fluorescence spectra of Trp-314 and Trp-15. Table II compares the spectral characteristics obtained by Abdallah et al. (1978) by means of selective quenching resolution with the present data by means of lifetime resolution.

Quenching in the NAD$^+$–Pyrazole Complex. Additional support for our tryptophan lifetime assignments is obtained from the decay kinetics of the NAD$^+$–pyrazole ternary complex. The *selective* quenching of the 3.8-ns component, associated with Trp-314, can readily be explained by singlet–singlet energy transfer. The characteristic absorption band

Table II: Fluorescence Spectral Parameters for Trp-15 and Trp-314

residue	steady-state fluorescence[a] ϕ	λ'_{max} (nm)	$\Delta\lambda$ (nm)	overlap,[b] J [(cm^6 mmol^{-1}) × 10^{-16}]
Trp-15	0.19	340 (337)	52 (54)	2.99
Trp-314	0.37	320 (324)	44 (43)	7.09

[a] Steady-state parameters (0.1 M phosphate pH 7.5 buffer, 23 °C) from Abdallah et al. (1978); our values, given in parentheses, are calculated from the fluorescence decay parameters according to eq 13. [b] The overlap integrals, using our lifetime-resolved emission spectra for the two tryptophans, each normalized to unity, were calculated from the extinction due to the NAD$^+$–pyrazole ternary complex less the absorbance due to ADH alone. Values for α_1 and α_2, below 310 nm, were extrapolated from the curves in Figure 2. The absorption spectrum of the ternary complex was identical with that determined by Theorell & Yonetani (1963).

which, as described by Theorell & Yonetani (1963), is due to formation of this particular complex, overlaps with the ADH tryptophan fluorescence and thus represents a potential acceptor. The overlap integrals for Trp-314 and Trp-15, based on the spectral distribution of the lifetime components and the absorption band due to formation of the NAD$^+$–pyrazole complex, are given in Table II.

Possible quenching of Trp-15 and Trp-314 by energy transfer to NAD$^+$–pyrazole within one subunit and from one subunit to the other was calculated with the use of eq 9–11. The refractive index was taken as 1.5. The distances between each tryptophan and the actives sites were obtained from Eklund et al. (1976).[2] The distance of Trp-15 to the active site on the same subunit is 27 Å and to the site on the other subunit is 60 Å. The distance of Trp-314 to the active site on the same subunit is 17 Å and to the site on the other subunit is 22 Å. The quantum yields of Abdallah et al. (1978), listed in Table II, were corrected for temperature according to our lifetime data, which gave values of 0.21 for Trp-15 and 0.41 for Trp-314. In all interactions κ^2 was assumed to have a value of 0.2 (κ^2 may vary from 0 to 4). Thus, the calculated R_0 values were 14.7 Å for Trp-314 and 11.4 Å for Trp-15. Accordingly, the transfer efficiency for Trp-15 is 0.01 for the same subunit and effectively 0 for the other subunit. And for Trp-314 it is 0.30 for the same subunit and 0.08 for the other subunit. Thus the expected quenching of Trp-15 is 1% and that of Trp-314 is 38%. It should be noted that there is very little quenching from one subunit to the other. According to our data, the transfer efficiency from Trp-15 is effectively 0 since there is no quenching of the long component. On the other hand, the transfer efficiency from Trp-314 would be ~37%.

The estimate of quenching due to energy transfer agrees with the experimentally observed decrease in the short decay time of the ternary complex. Therefore, a reasonable conclusion is that the selectivity in the quenching by NAD$^+$–pyrazole ternary complex formation has its origin in both the relative distances and the spectral overlaps between the NAD$^+$–pyrazole absorption and the Trp-15 and Trp-314 fluorescence.

Local Environments of Trp-314 and Trp-15. As discussed in the preceding paper (Ross et al., 1981), there is a marked

[2] The distances are computed from the midpoint of the aromatic ring systems of the tryptophan and the nicotinamide rings. If the distances are calculated to the adenine ring system, then the energy transfer from Trp-15 is <1% and the energy transfer from Trp-314 decreases from 38% to 32%.

variation in the limiting zero-time anisotropy, r_0, of tryptophan or NATA over the excitation region from 290 to 300 nm, the bandwidth of the excitation light used in our experiments. Since Trp-15 and Trp-314 have nonidentical absorption spectra, their r_0 values will likely be different at 295 nm, the excitation maximum of the filter in combination with the nitrogen lamp. The r_0 value of ~0.20 for ADH is therefore an average of the r_0 values of both tryptophan residues weighted by the relative fluorescence contribution of each residue. The single time constant for the decay of the anisotropy means that the motions of the exposed and buried tryptophans in the dimer are indistinguishable and all the indole rings are firmly bound to the protein matrix during the lifetime of the excited state. The slight increase in molecular volume could imply that there is a general "loosening" of the inter- and intramolecular interactions stabilizing the two polypeptide chains. However, up to 40 °C there is no obvious change in the mobility of Trp-15 or Trp-314.

To find possible reasons for the lack of mobility of the two tryptophans, we examined the 2.4-Å X-ray crystal structure model of ADH by Brändén and coworkers (Eklund et al., 1974, 1976). Several features are evident that are consistent with our results. Trp-314 is largely surrounded by hydrophobic or neutral residues. Of particular interest is a possible close interaction with the sulfur atom of Met-803 on the second subunit. In the excited singlet state of Trp-314, the spin–orbit interaction [cf. McGlynn et al. (1969)] enhanced by the heavy sulfur atom of Met-803 could account for the "short" lifetime of 3.8 ns. Increased spin–orbit coupling due to a shift in conformation in the NAD^+–pyrazole ternary complex could also be invoked to explain some of the additional fluorescence quenching. Apparently, singlet–singlet energy transfer cannot entirely account for the Trp-314 quenching in the NAD^+–trifluoroethanol ternary complex (Laws & Shore, 1978). In these two cases NAD^+ is the acceptor. Laws & Shore (1979), on the basis of difference absorption spectra, have suggested that the quenching at neutral pH is due to energy transfer to Tyr-286 ionized in the ground state. However, Subramanian et al. (1981) suggest that the difference absorption is not due to phenolate but rather to a probable charge interaction between an arginine residue and the adenine ring in the apparently low dielectric environment of the coenzyme binding pocket.

Since Trp-15 is on the surface of the enzyme, as is clearly evident from our KI quenching data as well as those of Abdallah et al., (1978), we were interested to find no fluctuations associated with this residue. We supposed that a strong interaction with the indole nitrogen might help immobilize the ring. A good candidate would be the side chain of an acidic residue. Upon examination of the crystal structure, we found that the carboxylic oxygens of Glu-24 are ~3 Å away from the indole nitrogen, certainly close enough to hydrogen bond to the NH group. Such an interaction could lead to static quenching of a fraction of the Trp-15 residues. This would be consistent with the small quantum yield (Abdallah et al., 1978) but long lifetime when compared with that of Trp-314. Measurement of the fluorescence decay at low pH, near the pK of the carboxyl side chain, would obviously be of interest. Unfortunately, the enzyme loses its zinc atoms and denatures below pH 6 (Vallee & Hoch, 1957).

That the fluorescence decay kinetics of Trp-15 and Trp-314 can be considered as single exponentials can reasonably be explained by the argument that both tryptophans reside in highly restricted environments. The indole rings would thus experience a sufficiently narrow range of interactions with the neighboring side groups such that no kinetically distinct "second" environment would exist. For example, the single highly mobile tryptophan in ACTH-(1–24) exhibits multiexponential decay kinetics for both the fluorescence and its anisotropy (Ross et al., 1981).

In agreement with the results of Lakowicz & Cherek (1980), we find that the mean decay time of the tryptophan fluorescence of ADH increases with increasing wavelength across the emission band. While this result is consistent with the notion of solvent relaxation around tryptophan, we have shown here that the data are better explained by assignment of the two decay times to the two tryptophan residues whose fractional emission varies with wavelength.

Acknowledgments

We thank Professors Joseph Lakowicz, Mary Barkley, Kenneth Rousslang, and Robert DeToma for their contributions toward some of the ideas developed in this paper. We also thank Dr. Philip Ross, Dr. Knut Hildenbrand, and Dr. Edward Jablonski for numerous discussions. Professor David C. Teller kindly measured the viscosity of our buffer. Richard Feldmann, of the National Institutes of Health, generously provided us with computer models generated from the 2.4-Å X-ray crystal structure coordinates of ADH (Eklund et al., 1974). Finally, we express our gratitude to Susan Thomas and Dana Walbridge for their help in computer programming and instrumentation and to Susan Jenkins and Linda Hall for help with the manuscript.

References

Abdallah, M. A., Biellman, J.-F., Wiget, P., Joppich-Khun, R., & Luisi, P. L. (1978) *Eur. J. Biochem. 89*, 397–405.

Azumi, T., & McGlynn, S. P. (1962) *J. Chem. Phys. 37*, 2413–2420.

Badea, M. G., & Brand, L. (1979) *Methods Enzymol. 61*, 378–425.

Badea, M. G., DeToma, R. P., & Brand L. (1978) *Biophys. J. 24*, 197–212.

Barboy, N., & Feitelson, J. (1978) *Biochemistry 17*, 4923–4926.

Brändén, C.-I., Jornvall, H., Eklund, H., & Furugren, B. (1975) *Enzymes, 3rd Ed. 11*, 103–190.

Chen, L. A., Dale, R. E., & Brand, L. (1977) *J. Biol. Chem. 252*, 2163–2169.

Dale, R. E., Chen, L. A., & Brand, L. (1977) *J. Biol. Chem. 252*, 7500–7510.

Dalziel, K. (1957) *Acta Chem. Scand. 11*, 397–398.

DeToma, R. P., Easter, J. H., & Brand, L. (1976) *J. Am. Chem. Soc. 98*, 5001–5007.

Donzel, B., Gauduchon, P., & Wahl, P. (1974) *J. Am. Chem. Soc. 96*, 801–808.

Easter, J. H., DeToma, R. P., & Brand, L. (1976) *Biophys. J. 16*, 571–583.

Einstein, A. (1906) *Ann. Phys. (Leipzig) 19*, 371–381, as referenced in (1956) *Investigations on the Theory of the Brownian Movement*, Dover Publications, New York.

Eisinger, J. (1969) *Biochemistry 8*, 3902–3908.

Eklund, H., Nordström, B., Zeppezauer, E., Soderland, G., Ohlsson, I., Boiwe, T., & Brändén C.-I. (1974) *FEBS Lett. 44*, 200–204.

Eklund, H., Nordström, B., Zeppezauer, E., Söderland, G., Ohlsson, I., Boiwe, T., Söderberg, B.-O., Tapia, O., Brändén, C.-I., & Åkeson, Å. (1976) *J. Mol. Biol. 102*, 27–59.

Förster, T. (1948) *Ann. Phys. (Leipzig) 2*, 55–75.

Förster, T. (1951) *Fluoreszenz organischer verbindungen*, Vandenhoeck and Reprecht, Gottingen.

Gafni, A., Modlin, R. L., & Brand, L. (1975) *Biophys. J. 15*, 263–280.
Gafni, A., Modlin, R. L., & Brand, L. (1976) *J. Phys. Chem. 80*, 898–904.
Grinvald, A., & Steinberg, I. Z. (1974) *Anal. Biochem. 59*, 583–598.
Grinvald, A., & Steinberg, I. Z. (1976) *Biochim. Biophys. Acta 427*, 663–678.
Inokuti, M., & Hirayama, F. (1965) *J. Chem. Phys. 43*, 1978–1989.
Konev, S. V. (1967) *Fluorescence and Phosphorescence of Proteins and Nucleic Acids*, Plenum Press, New York.
Lakowicz, J. R., & Cherek, H. (1980) *J. Biol. Chem. 255*, 831–834.
Laws, W. R., & Shore, J. (1978) *J. Biol. Chem. 253*, 8593–8597.
Laws, W. R., & Brand, L. (1979) *J. Phys. Chem. 83*, 795–802.
Lehrer, S. S. (1971) *Biochemistry 10*, 3254–3263.
McGlynn, S. P., Azumi, T., & Kinoshita (1969) *Molecular Spectroscopy of the Triplet State*, Prentice-Hall, Englewood Cliffs, NJ.
Munro, I., Pecht, I., & Stryer, L. (1979) *Proc. Natl. Acad. Sci. U.S.A. 76*, 56–60.
Paoletti, J., & Le Pecq, J.-B. (1969) *Anal. Biochem. 31*, 33–41.
Perrin, F. (1934) *J. Phys. Radium 5*, 497–511.
Perrin, F. (1936) *J. Phys. Radium 7*, 1–11.
Privat, J.-P., Wahl, P., & Auchet, J.-C. (1980) *Biophys. Chem. 11*, 239–248.
Purkey, R. M., & Galley, W. C. (1970) *Biochemistry 9*, 3569–3575.
Rigler, R., & Ehrenberg, M. (1973) *Q. Rev. Biophys. 6*, 139–199.
Ross, J. B. A., Rousslang, K. W., & Brand, L. (1981) *Biochemistry* (preceding paper in this issue).
Rousslang, K. W., Ross, J. B. A., Deranleau, D. A., & Kwiram, A. L. (1978) *Biochemistry 17*, 1087–1092.
Rousslang, K. W., Thomasson, J. M., Ross, J. B. A., & Kwiram, A. L. (1979) *Biochemistry 18*, 2296–2300.
Schiller, P. (1972) *Proc. Natl. Acad. Sci. U.S.A. 69*, 975–979.
Small, E. W., & Isenberg, I. (1977) *Biopolymers, 16*, 1907–1928.
Subramanian, S., Ross, J. B. A., Ross, P. D., & Brand, L. (1981) *Biochemistry 20*, 4086–4093.
Sund, H., & Theorell, H. (1963) *Enzymes, 2nd Ed. 7*, 25–67.
Tao, T. (1969) *Biopolymers 8*, 609–632.
Theorell, H., & Yonetani, T. (1963) *Biochem. Z. 338*, 537–553.
Torikata, T., Forster, L. S., O'Neal, C. C., & Rupley, J. A. (1979) *Biochemistry 18*, 385–390.
Vallee, B. L., & Hoch (1957) *J. Biol. Chem. 225*, 185–189.
Wahl, P. (1969) *Biochim. Biophys. Acta* 175, 55–64.

Identification of Novel 7,12-Dimethylbenz[*a*]anthracene Adducts in Cellular Ribonucleic Acid†

Krystyna Frenkel,‡ Dezider Grunberger,* Hiroshi Kasai, Hajime Komura, and Koji Nakanishi

ABSTRACT: The interaction of guanosine with 7,12-dimethylbenz[*a*]anthracene (DMBA) 5,6-oxide under alkaline conditions resulted in the formation of six derivatives. These six compounds were cochromatographed with nucleosides obtained by hydrolysis of RNA isolated from rat liver cells treated with [^{3}H]DMBA. The cochromatography showed that three of these adducts were formed in cellular RNA. The three products constituted less than 5% of the total nucleoside–DMBA adducts as shown by chromatography on Sephadex LH-20 and high-pressure liquid chromatography. In one of them, the 2′-hydroxy group of the ribose moiety of guanosine was linked to the C-5, and in the second, to the C-6 position of the DMBA 5,6-oxide residue. In the third derivative, the C-8 position of guanosine was linked to the C-5 of the DMBA 5,6-oxide moiety. These results show, for the first time, modifications of the ribose moiety and of the guanine residue at the C-8 position in the cellular RNA by a metabolite of a polycyclic hydrocarbon.

7,12-Dimethylbenz[*a*]anthracene (DMBA),[1] one of the most potent carcinogenic polycyclic aromatic hydrocarbons (Brookes & Lawley, 1964; Slaga et al., 1974), is metabolized to K-region and non-K-region dihydro diols and oxides before it reacts with nucleic acids (Sims, 1967; Keysell et al., 1973; Dipple & Nebzydoski, 1978; Tierney et al., 1978; Chou & Yang, 1978; McNicoll et al., 1980). Studies using mouse skin and embryo cells (Moschel et al., 1977; Bigger et al., 1978), hamster embryo cells (Ivanovic et al., 1978), or mouse fibroblasts (Marquardt et al., 1976) indicate that generation of the bay region diol epoxide (the C-1 to C-4 positions of DMBA) is required for formation of the majority of adducts with DNA. However, Cooper et al. (1980) have shown that in addition to the bay region diol epoxides there are other DMBA intermediates which bind to the DNA of mouse skin. Similarly, recent experiments with fluorinated derivatives of DMBA

† From the Cancer Center/Institute of Cancer Research, Department of Biochemistry, Columbia University College of Physicians & Surgeons (K.F. and D.G.), and the Department of Chemistry, Columbia University (H.K., H.K., and K.N.), New York, New York 10032. *Received December 18, 1980.* Dedicated to the late Professor František Šorm. Supported by Grants CA 21111, CA 13696, and CA 11572 from the National Cancer Institute, Department of Health and Human Services.
‡ Present address: Department of Pathology, New York University Medical Center, New York, NY.

[1] Abbreviations used: DMBA, 7,12-dimethylbenz[*a*]anthracene; DMBA oxide, DMBA K-region oxide, 7,12-dimethylbenz[*a*]anthracene 5,6-oxide; $NaDodSO_4$, sodium dodecyl sulfate; HPLC, high-pressure liquid chromatography.

0006-2960/81/0420-4377$01.25/0